Coherent Exciton Delocalization in a Two-State DNA-Templated Dye Aggregate System

Brittany L. Cannon[†], **Donald L. Kellis**[†], **Lance K. Patten**[†], **Paul H. Davis**[†], **Jeunghoon Lee**[†,‡], **Elton Graugnard**[†], **Bernard Yurke**[*,†,§], **William B. Knowlton**[*,†,§]

[†]Micron School of Materials Science & Engineering, Boise State University, Boise, Idaho 83725, United States

[‡]Department of Chemistry & Biochemistry, Boise State University, Boise, Idaho 83725, United States

[§]Department of Electrical & Computer Engineering, Boise State University, Boise, Idaho 83725, United States

Abstract

Coherent exciton delocalization in dye aggregate systems gives rise to a variety of intriguing optical phenomena, including J- and H-aggregate behavior and Davydov splitting. Systems that exhibit coherent exciton delocalization at room temperature are of interest for the development of artificial light-harvesting devices, colorimetric detection schemes, and quantum computers. Here, we report on a simple dye system templated by DNA that exhibits tunable optical properties. At low salt and DNA concentrations, a DNA duplex with two internally functionalized Cy5 dyes (i.e., dimer) persists and displays predominantly J-aggregate behavior. Increasing the salt and/or DNA concentrations was found to promote coupling between two of the DNA duplexes via branch migration, thus forming a four-armed junction (i.e., tetramer) with H-aggregate behavior. This H-tetramer aggregate exhibits a surprisingly large Davydov splitting in its absorbance spectrum that produces a visible color change of the solution from cyan to violet and gives clear evidence of coherent exciton delocalization.
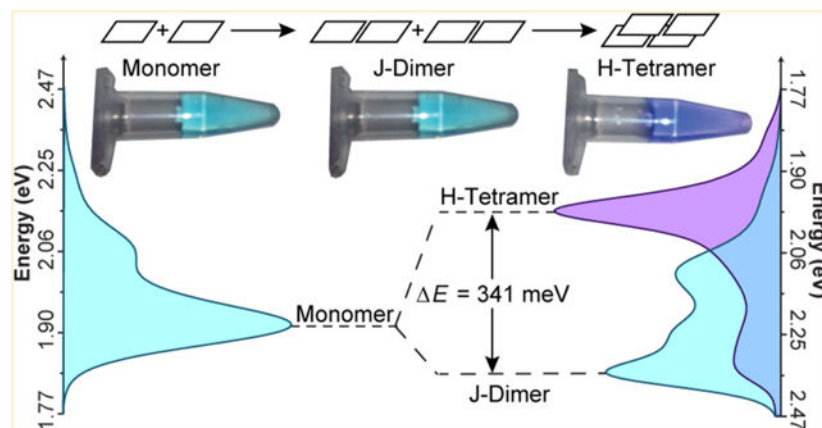
Graphical Abstract

INTRODUCTION

Coherent exciton delocalization, the process by which excitons (i.e., electron–hole pairs) spread in a wavelike manner over spatially separated molecular dyes,[1–5] is an intriguing phenomenon that has attracted the interest of quantum computational theorists for the role it might play in photosynthesis.[5–11] Frenkel, Davydov, and Kasha[12–15] pioneered the theoretical description of exciton delocalization within molecular crystals and aggregates. Exciton delocalization in dye aggregate systems has been shown to exhibit itself in a wide variety of optical phenomena, including Dicke super-radiance,[16–18] Davydov splitting, [12,13,19–21] and its more specific manifestations: J- and H-aggregate behavior,[22–39] superquenching,[28,40] exchange narrowing,[41,42] superfluorescence,[43,44] resonance fluorescence,[45–47] and excitonically coupled circular dichroism (EC-CD),[26,48] many of which depend strongly on the geometrical configuration of the dye aggregates. Shown in Figure 1, coherent coupling between two dyes results in a splitting of the excited state energy levels for which the allowed energy transitions, and thus optical properties are strikingly different depending on whether the dye molecules undergo head-to-tail stacking (referred to as J-aggregates, Figure 1a) or parallel stacking (referred to as H-aggregates, Figure 1b). In particular, J-aggregates, first observed by Jelley[49,50] and Scheibe,[51–53] exhibit a bathochromic (red) shift in absorbance, while H-aggregates exhibit a hypsochromic (blue) shift in absorbance relative to the monomeric dye. J-aggregates have been shown to produce a nearly resonant fluorescence emission (i.e., very small Stokes shift), yielding a high-intensity, sharp emission peak that can be exploited for the development of nonlinear optical devices,[30] light-harvesting systems,[54] and biological probes.[22,54] Conversely, H-aggregates have been used primarily as biological markers[35,37,55,56] due to a significantly reduced fluorescence emission intensity accompanied by a very large Stokes shift that arises from an optically forbidden energy transition. Intermediate geometrical configurations, termed oblique, exhibit a resonant band (Davydov) splitting of the absorbance spectrum that reflects a mixture of J- and H-aggregate optical properties resulting from the dye stacking geometry.[20]

Currently, coherent exciton delocalization is being explored in naturally occurring photosynthetic systems as a highly efficient energy transfer mechanism at ambient

temperatures.[6,10,11,57–59] Within these light-harvesting systems, proteins organize groups of chromophores (i.e., optically active dye) into aggregates with nearest-neighbor distances of 1–2 nm or less, which is necessary to induce and sustain coherence.[59] Mimicking intricate protein and dye interactions found within photosynthetic light-harvesting systems to assemble dye aggregates in a manner that promotes exciton delocalization has proven difficult owing to the complexity of protein folding mechanisms and dye–protein interactions.[8,60] An alternative approach is to use DNA as the biomolecular scaffold. Largely because of Watson–Crick base pairing and the linear structure of DNA oligomers, DNA assembly follows simple design rules. In addition, DNA can be easily labeled (i.e., functionalized) with an assortment of dye species using various dye attachment methods that enable proximal positioning of the dyes, thereby facilitating coherent interactions.[40,61]

Covalent attachment of dyes onto DNA oligomers[26,48,62–65] enables precise control of aggregate size and specificity of the covalent attachment site as well as offers a simple method for investigating the effects of dye surroundings on dye–dye interactions and the preferred aggregation stacking arrangement. As already established by Markova et al., two cyanine-based Cy5 dyes (see Supporting Information S1) covalently bound within a DNA duplex form a J-dimer while in the presence of 100 mM sodium chloride (NaCl).[26] In our work, we investigate the transition of J-type to H-type aggregate constructs at high salt and/or DNA concentrations through theoretical fitting of the spectral data, gel electrophoresis, and reaction kinetics studies, which supports the coupling of two J-dimers to form an H-tetramer by the combination of two DNA duplexes into a four-armed junction (4AJ). Strictly speaking, the DNA-templated J-dimers and H-tetramers are chiral oblique aggregates, as evidenced by our circular dichroism (CD) data, but exhibit predominantly J- or H-characteristics, respectively. Within the bulk solution, the equilibrium population ratios between the two aggregate states (i.e., J-dimer/duplex and H-tetramer/4AJ) are adjusted by varying the salt and DNA concentrations, thereby enabling control of the optical properties. In particular, for this two-state system, the large Davydov splitting (103 nm, 336 meV) manifested in the absorption spectra gives rise to vivid color changes as a result of the large separation between the two absorption peaks, establishing a distinct and visible signature of exciton delocalization.[66] Exploiting this unique DNA-templated method for discretely switching between aggregate states and precisely controlling the optical properties of the system provides a viable platform for the development of excitonic-based optoelectronic devices toward artificial light-harvesting systems, novel colorimetric detection schemes, and quantum computation.[8,9]

THEORETICAL ANALYSIS OF OPTICAL SPECTRA FOR STRUCTURAL MODELING

To extract structural information from the experimental data, theoretical absorbance and CD spectra were computed for various dye configurations and compared with the experimental spectra. The theoretical calculations proceeded by constructing a system Hamiltonian following a generalized approach guided by Kühn, Renger, and May that considers the case of N dye molecules having arbitrary positions and orientations.[67–71] This approach, which we will term the Kühn–Renger–May (KRM) model from here on, avoids any perturbational

treatment of the exciton–vibrational coupling. The energy eigenvalues and eigenvectors of this Hamiltonian were computed on a truncated Hilbert space. The construction of the Hamiltonian and the truncation of the Hilbert space are described in Supporting Information S2. Since the distance between the dyes is expected to be less than the length of the molecules, to achieve a better approximation rather than model the exciton exchange interaction as that between a pair of point dipoles, each dipole is modeled as a pair of opposite charges separated by a distance comparable to that of the length of the molecule (Supporting Information S2). The optical transition probabilities were computed for each eigenstate, and smooth absorption and CD spectra were obtained by convolving the transition probability line spectra with a Gaussian line shape, thereby approximating the effect of the vibronic continuum on spectral line shape. The absorbance and CD data were simultaneously fit to match the two dominant peaks of the absorption and CD spectra and obtain a generally good qualitative agreement for the shape of the spectra. The purpose of the KRM modeling is to obtain quantitative information regarding the dye stacking positions and orientations. From a qualitative inspection of the experimental data, it may be apparent that the dyes do not stack strictly in head-to-tail J-aggregate or face-to-face H-aggregate configurations, but it is not possible to determine the actual configurations that the structures will adopt.

Kinetics and Thermodynamics of the Two-State Model.

As will be highlighted when discussing the results of the reaction kinetics and thermodynamic studies of the system, the model that best describes the data is a second-order reaction in which two J-dimers reversibly combine to form an H-tetramer. This model is also corroborated by the theoretical fitting of optical spectra, which shows two J-dimer duplexes that couple together to form a 4AJ with four dyes (i.e., a tetramer) exhibiting predominantly H-aggregate behavior. Here, the model is described in detail.

Two-State Second-Order Reaction Kinetics Model.

The system in this study can be characterized by the following isothermal chemical reaction:

$$[J] + [J] \underset{k_{H \to J}}{\overset{k_{J \to H}}{\rightleftharpoons}} [H] \quad (1)$$
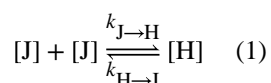
where [J], [H], $k_{J \to H}$, and $k_{H \to J}$ represent J-dimer and H-tetramer concentrations, the reaction rate constant for J-dimers combining to form H-tetramers (i.e., forward reaction), and the reaction rate constant for H-tetramers dissociating into pairs of J-dimers (i.e., reverse reaction), respectively. A schematic illustration of the J-dimer to H-tetramer states is given in Figure 2. The transition occurs via a four-way branch migration process to form a Holliday junction-like structure with dyes located at the junction core.[72–82] Figure 2 also indicates that although the H-type configuration is treated as a single state in the two-state reaction kinetics model, it is depicted as undergoing internal rearrangements due to breathing and restacking of the DNA bases near the Holliday junction core. These arrangements occur on 1 μs to 1 s time scales and are fast compared to interconversion of J-dimers and H-tetramers.[79,80] The internal rearrangements in Figure 2 are shown as causing

either a horizontal or vertical displacement, or separation of the dyes, resulting in the formation of dye dimers. We hypothesize that the existence of these multiple internal states (i.e., dimers that result from horizontal or vertical displacement) largely accounts for the J-aggregate like feature of the H-tetramer absorbance spectrum that appears at 665 nm.

Here, we derive the equations following from eq 1 that were used to fit the experimental kinetics and thermodynamic data. The rate equations for such a system are

$$\frac{d[J]}{dt} = -2k_{J\rightarrow H}[J]^2 + 2k_{H\rightarrow J}[H] \quad (2)$$

and

$$\frac{d[H]}{dt} = k_{J\rightarrow H}[J]^2 - k_{H\rightarrow J}[H] \quad (3)$$

From eqs 2 and 3, it follows that

$$\frac{d[J]}{dt} + 2\frac{d[H]}{dt} = 0 \quad (4)$$

If, at time $t = 0$, $[J] = [J]_0$ and $[H] = [H]_0$, then upon integrating eq 4, the conservation of mass equation is found:

$$[H] = \frac{1}{2}([DNA] - [J]) \quad (5)$$

where [DNA] represents the total double-stranded DNA (dsDNA) concentration, which is constant and approximately equal to the sum of $[J]_0$ and $2[H]_0$. Solving for [J] in eq 5 and substituting into eq 3 gives a rate equation in terms of [H]:

$$\frac{d[H]}{dt} = k_{J\rightarrow H}([DNA] - 2[H])^2 - k_{H\rightarrow J}[H] \quad (6)$$

Integrating the rate equation[83] and solving for [H] yields

$$[H] = \frac{1}{2}[DNA] - \frac{\sqrt{q}}{4c}\left(\frac{1 + \alpha e^{-\sqrt{q}t}}{1 - \alpha e^{-\sqrt{q}t}}\right) + \frac{b}{4c} \quad (7)$$

where the constants in eq 7 are given in terms of the rate constants and DNA concentration by

$$a = -k_{H \to J}[DNA] \quad (8)$$
$$b = k_{H \to J}$$
$$c = 2k_{J \to H}$$

and

$$q = -4ac + b^2 = 8k_{J \to H}k_{H \to J}[DNA] + k_{H \to J}^2 \quad (9)$$

$$\alpha = \frac{2c[J]_0 + b - \sqrt{q}}{2c[J]_0 + b + \sqrt{q}} \quad (10)$$

Details pertaining to the full derivation can be found in Supporting Information S3.

Fitting Reaction Kinetics Data.

To reduce the number of parameters used when fitting the reaction kinetics data, the rate equations were examined in the long time limit (i.e., $t = \infty$) at which the reaction equilibrium is reached. Thus, from eq 7, one obtains the following:

$$[H]_{t = \infty} = \frac{1}{2}[DNA] - \frac{\sqrt{q}}{4c} + \frac{b}{4c} \quad (11)$$

Solving for 1/2[DNA] in eq 11 and substituting into eq 7, the $b/4c$ term is eliminated. Analyzing the newly simplified eq 7 at $t = 0$, one finds

$$[H]_{t = 0} = [H]_{t = \infty} - \frac{\sqrt{q}}{2c}\left(\frac{\alpha}{1 - \alpha}\right) \quad (12)$$

Rearranging eq 12 to solve for the $q/2c$ term and substituting into eq 7, the $q/2c$ term is eliminated, thus yielding the following:

$$[H] = \left([H]_{t = 0} - [H]_{t = \infty}\right)\left(\frac{(1 - \alpha)e^{-\sqrt{q}t}}{1 - \alpha e^{-\sqrt{q}t}}\right) + [H]_{t = \infty} \quad (13)$$

Because the α term is nearly zero (see Supporting Information Tables S4.1 and S4.2), eq 13 can be rewritten as

$$[H] = \left([H]_{t = 0} - [H]_{t = \infty}\right)\left(e^{-\sqrt{q}t}\right) + [H]_{t = \infty} \quad (14)$$

Thus, the fitting equation is equivalent to a decaying exponential function. To more accurately determine the rate constants, absorption spectra were obtained for completed reaction kinetics experiments performed at a variety of temperatures to ascertain the final concentrations of J-dimers and H-tetramers, thereby providing the equilibrium constant, K_{eq}, for the reaction at a series of temperatures. Expressing a in terms of K_{eq} and substituting into eq 13 eliminates one of the unknown variables in the fit, such that only three parameters (q, $[H]_{t=\infty}$, and $[H]_{t=0}$) are varied during the fitting procedure (eq 14).

The temperature-dependent rate constants appearing in eq 1 can be determined by evaluating reaction kinetics data obtained at different temperatures using eq 14. Assuming the reactions exhibit Arrhenius behavior, the activation energy and frequency factor for the forward (J → H) and reverse (H → J) reactions can then be calculated.

Effects of DNA Concentration on J- and H-Aggregate Populations.

Because of the second-order nature of the proposed reaction mechanism (eq 1), the direction of the reaction will be dependent on the DNA concentration, with formation of H-tetramers favored at high DNA concentration. Note that the effective dye concentration is proportional to the DNA concentration. Additionally, one can solve for a single population (i.e., [J] or [H]) by relating eq 5 to the equilibrium constant, K_{eq}:

$$K_{eq}[J]^2 = [H] = \frac{1}{2}([DNA] - [J]) \quad (15)$$

Rearranging eq 15 gives

$$2K_{eq}[J]^2 + [J] - [DNA] = 0 \quad (16)$$

Solving for [J] and disregarding the negative solutions leads to

$$[J] = \frac{\sqrt{1 + 8K_{eq}[DNA]} - 1}{4K_{eq}} \quad (17)$$

Similarly, [H] can be found to be

$$[H] = \frac{1}{2}\left([DNA] - \frac{\sqrt{1 + 8K_{eq}[DNA]} - 1}{4K_{eq}}\right) \quad (18)$$

Thus, using eqs 17 and 18, while conserving mass, the following relationships expressing the relative fractions of J-dimers and H-tetramers in solution can be obtained:

$$\frac{[J]}{[J] + 2[H]} = \frac{\sqrt{1 + 8K_{eq}[DNA]} - 1}{4K_{eq}[DNA]} \quad (19)$$

$$\frac{2[H]}{[J] + 2[H]} = 1 - \frac{\sqrt{1 + 8K_{eq}[DNA]} - 1}{4K_{eq}[DNA]} \quad (20)$$

RESULTS AND DISCUSSION

Optical Analysis of Dye-Aggregate States.

To optically characterize each dye-aggregate state and identify key coherent exciton delocalization spectral signatures, the absorbance, fluorescence, and CD spectra were measured for Cy5-DNA systems in $1\times$ TAE buffer with 0 mM $MgCl_2$ (J-dimer) and 155 mM $MgCl_2$ (H-tetramer) added at a DNA concentration of 1.5 μM (Figure 3). Spectral analysis of the dye monomer (Figure 3a) shows absorbance and emission peaks at 646 and 672 nm, respectively, yielding a 26 nm Stokes shift, which is in accordance with the literature values. [26,84] The full width at half-maximum (FWHM) of the absorbance (Abs) and fluorescence (FL) spectra were determined using a Gaussian fit to the data, as described further in Supporting Information S5. As expected, the monomer did not produce an observable CD signal in the visible region of the spectrum (Figure 3b), indicating molecular achirality and the absence of excitonic coupling. In contrast, the right-handedness of the β-DNA macromolecule structure gives rise to an anticipated chiral induced CD signal in the UV region. [85] Figure 3c, visualized using the UCSF Chimera software package, [86,87] depicts a possible representation of the monomer Cy5 internally functionalized onto a DNA duplex.

The J-dimer optical spectra presented in Figure 3d show similar spectral properties to those previously reported. [26] The J-dimer absorbance spectrum showed a peak at 665 nm that is red-shifted nearly 20 nm relative to that of the monomer (λ_{max} = 646 nm). Additionally, the J-dimer fluorescence maximum occurred at 667 nm, corresponding to an almost imperceptible (2 nm) Stokes shift relative to the absorption maximum. Both the absorbance and fluorescence peaks underwent a narrowing of the FWHM by ~20% compared to the monomer. The narrowing of the J-dimer absorbance peaks can be attributed to exchange narrowing (i.e., motional narrowing), [41] while the small Stokes shift and narrowing of the fluorescence peak are indicative of resonance fluorescence and consistent with J-aggregate behavior. [22,46,47] Both exchange narrowing and resonance fluorescence are optical responses consistent with excitonic delocalization. To further corroborate the nature of the J-dimer, Figure 3e reveals a biphasic visible CD spectrum indicative of an EC-CD phenomenon, which is also characteristic of exciton delocalization. The observed +/− of the CD peaks, moving from long wavelength (i.e., low energy) to short wavelength (i.e., high energy), indicates right-handedness. [48] The handedness of the J-dimer is most likely influenced by the right-handed β-DNA macromolecule.

From fitting of the absorbance and CD data to the KRM model, the relative distances and orientations between the Cy5 dyes can be predicted, thus providing the information necessary for visualizing the dye stacking arrangement of the J-dimer (Figure 3f). Fitting determined that the dyes are indeed stacked in a head-to-tail arrangement, as would be expected in a J-type aggregate, and oriented with a slight obliqueness that manifests itself in the optical spectra as an increase in the vibronic peak at 598 nm. Additionally, it was determined that the center-to-center distance between the two dyes is ~1.51 nm, with the closest distance between the two dye molecules being 0.37 nm. Fitting input parameters and output dye angles and positions are listed in Supporting Information Tables S2.1 and S2.2, respectively. The H-aggregate (Figure 3g) exhibited a substantially blue-shifted absorbance peak at 562 nm as compared to the monomer (646 nm). Because of the semimobility of the 4AJ, the H-tetramer is in rapid equilibrium with each of the asymmetrical four-armed structures composed of two J-dimers (Figure 2). The simultaneous presence of both the blue-shifted (H-aggregate behavior) and red-shifted (J-aggregate behavior) peaks, with respect to the monomer peak, is hypothesized to result from the combination of the rapid equilibrium between the two aggregate states (i.e., H-tetramer and J-dimers) and an obliqueness in the dye stacking arrangement. Though the obliqueness of the dye stacking is akin to Davydov splitting, the aggregate exhibits predominantly H-aggregate behavior. Here, the splitting is greater than 100 nm (~336 meV), which is quite large, leading to an observed color change of the solution from cyan (monomer/J-dimer) to violet upon formation of H-tetramers. Additionally, with an emission peak maximum at 666 nm, the system has a 104 nm Stokes shift relative to the blue-shifted absorbance peak. Similar to the J-dimer spectrum, the H-tetramer absorbance peak at 562 nm exhibited spectral narrowing (18 nm FWHM compared to the monomer peak's FWHM of 29 nm) as a consequence of exchange narrowing. The fluorescence peak intensity, when excited at the H-tetramer absorbance maximum (562 nm), was reduced by a factor of 4 relative to both the monomer and the J-dimer, as would be expected based on Kasha's molecular exciton theory for H-aggregates. [14,15]

Theoretical fitting of the H-tetramer absorbance and CD spectra (green dashed curves, Figure 3g,h) using the KRM model also provides insight into the orientation of the four dyes, which is schematically visualized in Figure 3i. The fitting input parameters and output dye angles and positions for the best fit are listed in Supporting Information Tables S2.1 and S2.2, respectively. It was found that the dyes are positioned such that three dyes stack in a nearly parallel fashion with ~0.4 nm separation, while the fourth dye stacks at an angle relative to the other dyes and with a somewhat greater nearest-neighbor separation. The variation in the orientation and spacing of the dyes relative to one another may occur due to strain within the 4AJ core. The best fit absorbance spectrum displays two peaks: one at 462 nm, which matches the experimental absorbance peak, and the other at 650 nm, which does not quite match the experimental red-shifted peak at 665 nm (Figure 3g). The obliqueness of this stacking arrangement enables a good fit of the KRM model to the observed EC-CD signal (Figure 3h). Interestingly, the CD spectrum reveals a −/+ biphasic signal, which is indicative of a left-handed excitonically coupled structure. The left-handedness of the dye stacking arrangement suggests that the dye aggregate is not influenced directly by the immediate DNA macromolecule structure, which is right-handed. Rather, the handedness

most likely arises from the formation of the larger 4-armed DNA construct. Curiously, a positive Cotton effect[88] (i.e., right rotation of circularly polarized light) also appeared at 317 nm, within the range of the DNA signal, for the H-tetramer. This may be related to interactions between the DNA and Cy5 dyes or result from the formation of the 4-armed structure.

The shape of the experimental absorbance spectrum in the 650–700 nm range is similar to that of the dimer absorption spectrum, which suggests that the contribution at this end of the spectrum is due to internal rearrangements of the Holliday junction core in which dyes are paired as depicted in Figure 2. The experimental absorbance spectrum is a sum of the absorbance spectra of the individual core states. The discrepancy between the experimental and best fit absorbance spectra in this spectral region may thus be the result of attempting to find a single structure that best fits the spectrum produced by an ensemble of structures. A more rigorous test of the KRM model would require a reliable means by which to determine what the individual contribution is of each core state to the absorbance and CD spectra.

Investigation of Aggregation State Reaction Kinetics and Thermodynamics.

To enhance our understanding of the reaction by which H-tetramer formation occurs, the kinetics and thermodynamics of the transition between J-dimer and H-tetramer states were investigated. The procedure used to obtain reaction kinetics spectra as a function of time and temperature is illustrated in Figure 4a,b and described in detail in Supporting Information S4. Reaction kinetics data (Figure 4c,d) were obtained by exploiting the H-tetramer absorbance peak at 562 nm to monitor aggregate state changes with minimal spectral interference from the monomer absorbance centered at 645 nm. Data were collected at several temperatures and fit to eq 14 to extract the rate constants. The average rate constants ($k_{J \rightarrow H}$ and $k_{H \rightarrow J}$) at each temperature were computed and are listed in Supporting Information Tables S4.3 and S4.4. Figure 4c,d shows representative data sets (circles, squares, etc.) fit to eq 14 using the averaged rate constants (black curves). Our extracted rate constants were found to be relatively slow and on the order of 10^{-2}–10^{-4} s^{-1} and 10^{-5}–10^{2} M^{-1} s^{-1} for $k_{J \rightarrow H}$ and $k_{H \rightarrow J}$, respectively. Additionally, it was observed that increasing the temperature of the system by 10 °C led to a 2 orders of magnitude increase in the reaction rate constants, which exhibited Arrhenius-type behavior. The slow rate of the reaction would be expected for a case in which two DNA duplexes undergo four-way branch migration to form a 4AJ. Specifically, the magnesium ions present in solution, as opposed to monovalent sodium ions, have been shown to slow the rate of reaction.[77,89]

Plotting the log of the averaged rate constants against the inverse of temperature, the activation energies (listed in Table 1) for the aggregation state transitions were calculated using a linear fit (Figure 4e,f). The reported values for activation energies of the dimerization of free-floating dyes are typically a factor of 4 smaller than what we report in Table 1.[90] However, this composite two-state system consists of both dyes and DNA oligomers and thus is expected to exhibit strong temperature dependence due to physical processes such as DNA breathing and macromolecular rearrangement. A deeper understanding of the activation energy and frequency factor values will require structural

and molecular dynamic information on the process leading to the transformation of a pair of J-dimers into an H-tetramer.

To calculate the free energy of the system, the Gibbs Free energy ($\Delta G°$) was computed as described in Supporting Information S7. The $J_0 \rightarrow H93.75$ reaction, in which two J-dimers (duplexes) combine to form an H-tetramer (4AJ), has a $\Delta G°$ of −22.5 kJ/mol, while the $H_{100} \rightarrow J_{6.25}$ reaction, in which an H-tetramer dissociates into two J-dimers, has a $\Delta G°$ value of +7.1 kJ/mol (Table 1). Because the system's entropy decreases with the formation of an H-tetramer and increases with the dissociation of H-tetramers into J-dimers, we can extrapolate that the enthalpy of the system must be negative for $J_0 \rightarrow H93.75$ transitions and positive for $H_{100} \rightarrow J_{6.25}$ transitions in the temperature range studied. The relatively small $\Delta G°$ values are consistent with our hypothesis of 4AJ formation due to similar base-pairing energy of the two states. Thus, the differences in the free energy arise primarily from dye−dye interactions and the change in configurational entropy.[77]

On the basis of the outcome of the spectral fitting using the KRM model (Figure 3) and the success of the second-order reaction kinetics model in fitting the reaction kinetics data (Figure 4), it was hypothesized that the H-tetramer consisted of a complex having four duplex arms extending from the central core, and thus should exhibit mobility, under nondenaturing gel electrophoresis conditions, comparable to that of a four-armed Holliday junction with arms of the same length (Figure 4g,h). These expectations were confirmed by gel shift experiments in which the mobility of the H-tetramer was compared with that of a Holliday junction and an assortment of controls. Details of the experiments and multiarmed DNA structure designs are provided in Supporting Information S6.1. The results show (0 mM $MgCl_2$, Figure 4g) that the J-dimer (lane 4) migrates through the gel at a mobility rate similar to that of the duplex structures (lanes 1–3), indicating that a duplex persists without higher-ordered aggregation. As expected for high salt concentration (100 mM $MgCl_2$, Figure 4h), the transport of the H-tetramer (lane 4) mimics the mobility of a four-armed structure (lane 6)—as opposed to smaller structures such as the duplexes (lanes 1–3) and three-armed construct (lane 5) or a larger structure such as the six-armed construct in lane 7. This structural information supports our hypothesis that the H-tetramer consists of two DNA duplexes combined to form a four-armed construct, stabilized by the four centrally located Cy5 dyes. The identities of the J-dimer (red box and corresponding absorbance curve) and H-tetramer bands (blue box and corresponding absorbance curve) were confirmed by excising the bands, eluting their contents, and measuring their respective absorbance curves (Figure 4i).

Overall, it was found that the proposed reaction kinetics model (eq 1) described the experimental reaction kinetics data extremely well (Figure 4c,d). An implication of the goodness of the fits of the data to a two-state second-order reaction kinetics model (eq 1) is that the size (i.e., order) of the dye aggregation is explicitly 2-fold and that higher-ordered aggregation (i.e., formation of multimers beyond H-tetramers) is not observed. Thus, unlike free-floating dyes that form large aggregates,[91–93] our dye–DNA system only forms small H-tetramer aggregates. The formation of H-tetramers, as opposed to larger aggregates such as H-hexamers, is further substantiated by the PAGE characterization (Figure 4g,h), which

explicitly correlates the mobility of the H-tetramer construct to that of a four-armed structure.

Effects of Salt and DNA Concentrations on J- and H-Aggregate Populations.

Precise arrangement of dye aggregates is essential for controlling excitonic delocalization behavior. Because it has been shown that both dye and salt concentration affect the aggregation of free-floating dyes,[49–53,91,92,94,95] we explored the effects of both salt and DNA concentrations on the preferred Cy5 dye stacking arrangements within our DNA-templated system to test the proposed reaction model (eq 1). Note that the DNA concentration is proportionate to the dye concentration and the salt concentration is explicitly added salt to a TAE buffer solution. After collecting the UV−vis absorbance spectrum of each sample (Figure 5a,b), the spectra of PAGE purified controls (see Supporting Information S8) were used to calculate the relative percentage of J- and H-aggregate populations present in solution at various salt (0–100 mM added $MgCl_2$) and DNA (0.1–10 μM) concentrations. Figure 5a,b shows that with changes in salt or DNA concentration the locations of the absorbance peaks remain constant within the selected $MgCl_2$ and DNA concentration ranges, respectively. The absence of variation in the position of the absorption peaks implies that the relative orientations between the two dyes are constant for the two populations, suggesting that the dyes do not continuously rearrange their configuration as a function of salt concentration or DNA concentration but instead exist in one of two geometrically distinct states, as a J-dimer (duplex) or an H-tetramer (4AJ). Accordingly, the relative concentration of each aggregate state varies with salt concentration and/or DNA concentration as indicated by the change in relative peak intensities for the J-dimer ($\lambda_{max} = 665$ nm) and the H-tetramer ($\lambda_{max} = 562$ nm). Furthermore, as shown in Supporting Information Figure S8.2, absorption spectra at intermediate salt or DNA concentrations are well approximated using a linear combination of the PAGE purified J- and H-aggregate spectra. Thus, the observed spectra are a manifestation of spectral overlap between J- and H-aggregates.

Using the fitting procedure described in Supporting Information S8.2, the relative populations of J- and H-aggregates can be determined. Figure 5c shows the changes in aggregate populations (taking into account conservation of mass) as a function of salt (i.e., added $MgCl_2$) concentration. Plotting the changes in ratio of J- to H-aggregates as a function of salt concentration revealed a sigmoidal-like trend in which higher $MgCl_2$ concentrations produced a favorable environment for H-tetramer formation (Figure 5c). The dye studied, Cy5, has been found to naturally arrange into H-aggregates at high salt and dye concentrations,[96] and recent studies from Mooi et al. show that the addition of ionic species can promote higher-ordered aggregation of cyanine-based dyes.[91,92] Furthermore, it is also known that an excess of Mg^{2+} can aid with neutralizing the negative charge of the DNA backbone, thereby decreasing the charge repulsion between adjacent DNA duplexes and allowing two J-dimers to interact within proximal distances. Thus, it is not surprising that the dye−DNA constructs tend to assemble into H-tetramers at these high ionic strengths. Figure 5d displays how the aggregate population composition changes with increasing DNA concentration. If the transformation between J- and H-aggregates were simply first order (as expected for dye conformational changes within a DNA duplex), changes would not be

observed in the relative concentrations of J-dimers ([J]) to H-tetramers ([H]) as a function of the DNA concentration, [DNA]. Furthermore, the percentages of J-dimers and H-tetramers present in solution, defined as [J]/([J] + 2[H]) and 2[H]/([J] + 2[H]), would be constants independent of [DNA]. The dependence of the relative populations of J- and H-aggregates on [DNA] provides a strong indication that a second-order reaction mechanism is involved, and agrees with previous studies that show aggregation is concentration dependent. [51–53,93,96,97] As shown by the fit line in Figure 5d, the observed trend correlates well with eqs 19 and 20, lending support for the proposed second-order reaction described by eq 1 and used to fit the data as demonstrated in Figure 4.

Distance Dependence of Coherent Exciton Delocalization.

Exciton delocalization results from strong excitonic coupling between neighboring dyes located with a spatial proximity of less than a few nanometers. [59] Because the dimensions of the DNA helix are well-known, varying the number of bps separating the Cy5 dye pair within the DNA construct provides a means for examining the dependence of the dye coupling strength on spatial separation (Figure 6).

In Figure 6, the absorbance spectra of the variable bp-separated dye-pairs are compared to the monomer (i.e., control), which shows a single peak at 646 nm with a small vibronic shoulder at 599 nm. At high salt concentration and 0 bp separation, the monomer peak at 646 nm is absent, while both a blue-shifted peak at 562 nm (characteristic of an H-aggregate) and a red-shifted peak at 665 nm (characteristic of J-aggregate behavior) appear simultaneously, consistent with Davydov splitting. The large Davydov splitting (103 nm) results in an observable color change of the solution from cyan (monomer) to violet, which is a visible indication of coherent exciton delocalization. Upon increasing the dye pair separation to 1 bp, the H-aggregate peak completely disappears, while the J-aggregate peak is only shifted slightly to 659 nm (i.e., 13 nm relative to the monomer rather than 19 nm as in the case of 0 bp separation), suggesting that H-tetramer formation is no longer favorable, and the coupling between the J-dimer dyes has weakened. The increase in the vibronic peak at 598 nm correlates well to the vibronic effects discussed by Spano with the formation of J-aggregates. [98] Increasing the distance to 2 bp separation returns the spectrum to that of the monomeric form, implying that coupling of the dyes has ceased. While these data test the variability of spatial separation along with dye orientation (i.e., resulting from the helical nature of the DNA template) and the local chemical environment (i.e., due to differences in neighboring base pairs), overall we find that the absorption spectrum profile of the dye aggregates with 2–4 bp separation reflect the shape of the monomer spectrum, indicating that spatial proximity has the greatest effect on the Davydov splitting. Moreover, the extremely large band splitting at relatively small (<2 nm) distances, in combination with both J- and H-aggregate optical behavior, corresponds well with models described by Kasha[14,15] and provides strong evidence for coherent exciton delocalization.

CONCLUSION

In this study, we have investigated excitonic delocalization in a DNA-templated dye aggregate system. Specifically, it was found that a Cy5 dye–DNA dimer construct, which

exhibits primarily J-aggregate characteristics at low salt and DNA concentrations, can couple with a second dimer to form a tetramer with predominantly H-aggregate characteristics at higher salt and/or DNA concentrations. Characterizing the reaction kinetics and subsequent thermodynamic equilibrium behavior of this two-state system combined with performing gel electrophoresis studies suggested that the H-tetramer formed through a branch migration process in which a four-armed DNA construct was assembled with four Cy5 dyes located centrally. The oblique stacking of these arrangements, as evidenced by EC-CD signals and validated by fitting the spectral data with the KRM model, results in a large Davydov splitting of the absorbance spectrum as well as a significant change of the solution color from cyan to violet. Furthermore, we show that the relative concentration of the two aggregate states (i.e., J-dimer versus H-tetramer) can be controlled by changing the salt and/or DNA concentrations, such that H-tetramer aggregates are favored at high salt and/or DNA concentrations. The large deviation we have observed in the absorption spectra of the J-dimer and H-tetramer configurations compared to that of the monomer indicates that further investigation of the use of DNA-templated dye aggregates with controlled structure is warranted. The development of precisely assembled dyes that exhibit exciton delocalization may enable the construction of aggregates in configurations that are not easily accessible in simple dye–solvent systems. The delocalization of excitons over such dye aggregates may allow the tailoring of absorption and fluorescence spectra for application in light harvesting, analysis of chemicals, and biological imaging. Advancing the development of DNA-templated dye aggregate systems even further by assembling complex networks of dyes to propagate exciton signals via coherent exciton exchange may enable information processing and perhaps quantum computing.

Supplementary Material

Refer to Web version on PubMed Central for supplementary material.

ACKNOWLEDGMENTS

REFERENCES

(1). Blancafort L; Voityuk AA Exciton Delocalization, Charge Transfer, and Electronic Coupling for Singlet Excitation Energy Transfer between Stacked Nucleobases in DNA: An MS-CASPT2 Study. J. Chem. Phys 2014, 140, 095102. [PubMed: 24606381]

(2). Scholes GD; Rumbles G Excitons in Nanoscale Systems. Nat. Mater 2006, 5, 683–696. [PubMed: 16946728]

(3). Monshouwer R; Abrahamsson M; vanMourik F; vanGrondelle R Superradiance and Exciton Eelocalization in Bacterial Photosynthetic Light-Harvesting Systems. J. Phys. Chem. B 1997, 101, 7241–7248.

(4). Lim JM; Kim P; Yoon MC; Sung J; Dehm V; Chen ZJ; Wurthner F; Kim D Exciton Delocalization and Dynamics in Helical Pi-Stacks of Self-Assembled Perylene Bisimides. Chem. Sci 2013, 4, 388–397.

(5). Dahlbom M; Pullerits T; Mukamel S; Sundström V Exciton Delocalization in the B850 Light-Harvesting Complex: Comparison of Different Measures. J. Phys. Chem. B 2001, 105, 5515–5524.

(6). Scholes GD Quantum Biology: Coherence in Photosynthesis. Nat. Phys 2011, 7, 448–449.

(7). Scholes GD; Fleming GR; Olaya-Castro A; van Grondelle R Lessons from Nature about Solar Light Harvesting. Nat. Chem 2011, 3, 763–774. [PubMed: 21941248]

(8). Engel GS Quantum Coherence in Photosynthesis. Procedia Chem. 2011, 3, 222–231.

(9). Saikin SK; Eisfeld A; Valleau S; Aspuru-Guzik A Photonics Meets Excitonics: Natural and Artificial Molecular Aggregates. Nanophotonics 2013, 2, 21–38.

(10). Ishizaki A; Fleming GR Quantum Coherence in Photo-synthetic Light Harvesting. Annu. Rev. Condens. Matter Phys 2012, 3, 333–361.

(11). Engel GS; Calhoun TR; Read EL; Ahn T-K; Mancal T; Cheng Y-C; Blankenship RE; Fleming GR Evidence for Wavelike Energy Transfer through Quantum Coherence in Photo-synthetic Systems. Nature 2007, 446, 782–786. [PubMed: 17429397]

(12). Davydov AS Theory of Absorption Spectra of Molecular Crystals; Institute of Physics, Academy of Sciences of Ukrainian SSR: Kyiv, Ukraine, 1948; Vol. 18.

(13). Davydov AS The Theory of Molecular Excitons. Soviet Physics 1964, 7, 145–178.

(14). Kasha M Energy Transger Mechanisms and Molecular Exciton Model for Molecular Aggregates. Radiat. Res 1963, 20, 55. [PubMed: 14061481]

(15). Kasha M; et al. The Exciton Model in Molecular Spectroscopy. Pure Appl. Chem 1965, 11, 371.

(16). Gross M; Haroche S Super-Radiance: An Essay on the Theory of Colective Spontaneous Emission. Phys. Rep 1982, 93, 301–396.

(17). Dicke RH Coherence in Spontaneous Radiation Processes. Phys. Rev 1954, 93, 99–110.

(18). Spano FC; Kuklinski JR; Mukamel S Temperature-Dependent Superradiant Decay of Excitons in Small Aggregates. Phys. Rev. Lett 1990, 65, 211–214. [PubMed: 10042581]

(19). Scholes GD; Ghiggino KP; Oliver AM; Paddonrow MN Through-Space and Through-Bond Effects on Exciton Interactions in Rigidly Linked Dinaphyl Molecules. J. Am. Chem. Soc 1993, 115, 4345–4349.

(20). Pajusalu M; Raetsep M; Trinkunas G; Freiberg A Davydov Splitting of Excitons in Cyclic Bacteriochlorophyll a Nanoaggregates of Bacterial Light-Harvesting Complexes between 4.5 and 263 K. ChemPhysChem 2011, 12, 634–644. [PubMed: 21275034]

(21). Zimanyi EN; Silbey RJ Theoretical Description of Quantum Effects in Multi-Chromophoric Aggregates. Philos. Trans. R. Soc., A 2012, 370 (1972), 3620–3637.

(22). Wuerthner F; Kaiser TE; Saha-Moeller CR J-Aggregates: From Serendipitous Discovery to Supramolecular Engineering of Functional Dye Materials. Angew. Chem., Int. Ed 2011, 50, 3376–3410.

(23). Wang MM; Silva GL; Armitage BA DNA-Templated Formation of a Helical Cyanine Dye J-Aggregate. J. Am. Chem. Soc 2000, 122, 9977–9986.

(24). von Berlepsch H; Bottcher C Supramolecular Structure of TTBC J-Aggregates in Solution and on Surface. Langmuir 2013, 29, 4948–4958. [PubMed: 23527663]

(25). Stiel H; Teuchner K; Becker W; Freyer W; Dahne S Fluorescence Lifetime Studies of Pseudoisocyanone J-Aggregates in the Subnanosecond Range. J. Mol. Struct 1984, 114 (3), 351–354.

(26). Markova LI; Malinovskii VL; Patsenker LD; Haner R J-vs. H-Type Assembly: Pentamethine Cyanine (Cy5) as a Near-IR Chiroptical Reporter. Chem. Commun 2013, 49, 5298–5300.

(27). Li ZA; Mukhopadhyay S; Jang S-H; Bredas J-L; Jen AKY Supramolecular Assembly of Complementary Cyanine Salt J-Aggregates. J. Am. Chem. Soc 2015, 137, 11920–11923. [PubMed: 26352648]

(28). Jones RM; Bergstedt TS; Buscher CT; McBranch D; Whitten D Superquenching and Its Applications in J-Aggregated Cyanine Polymers. Langmuir 2001, 17, 2568–2571.

(29). Iwaura R; Ohnishi-Kameyama M; Iizawa T Construction of Helical J-Aggregates Self-Assembled from a Thymidylic Acid Appended Anthracene Dye and DNA as a Template. Chem. - Eur. J 2009, 15, 3729–3735. [PubMed: 19206120]

(30). Herrera F; Peropadre B; Pachon LA; Saikin SK; Aspuru-Guzik A Quantum Nonlinear Optics with Polar J-Aggregates in Microcavities. J. Phys. Chem. Lett 2014, 5, 3708–3715. [PubMed: 26278740]

(31). Gadde S; Batchelor EK; Weiss JP; Ling YH; Kaifer AE Control of H- and J-Aggregate Formation via Host-Guest Complexation using Cucurbituril Hosts. J. Am. Chem. Soc 2008, 130, 17114–17119. [PubMed: 19007116]

(32). Fidder H; Knoester J; Wiersma DA Superradiant EMission and Optical Dephasing in J-Aggregates. Chem. Phys. Lett 1990, 171, 529–536.

(33). Ruedas-Rama MJ; Orte A; Martin-Domingo MC; Castello F; Talavera EM; Alvarez-Pez JM Interaction of YOYO-3 with Different DNA Templates to Form H-Aggregates. J. Phys. Chem. B 2014, 118, 6098–6106. [PubMed: 24837360]

(34). Ruedas-Rama MJ; Alvarez-Pez JM; Orte A Formation of Stable BOBO-3 H-Aggregate Complexes Hinders DNA Hybridization. J. Phys. Chem. B 2010, 114, 9063–9071. [PubMed: 20572644]

(35). Ikeda S; Okamoto A Hybridization-Sensitive On-Off DNA Probe: Application of the Exciton Coupling Effect to Effective Fluorescence Quenching. Chem. - Asian J 2008, 3, 958–968. [PubMed: 18446920]

(36). Asanuma H; Shirasuka K; Takarada T; Kashida H; Komiyama M DNA-Dye Conjugates for Controllable H* Aggregation. J. Am. Chem. Soc 2003, 125, 2217–2223. [PubMed: 12590550]

(37). Ikeda S; Kubota T; Kino K; Okamoto A Sequence Dependence of Fluorescence Emission and Quenching of Doubly Thiazole Orange Labeled DNA: Effective Design of a Hybridization-Sensitive Probe. Bioconjugate Chem. 2008, 19, 1719–1725.

(38). Armitage BA Cyanine Dye-DNA Interactions: Intercalation, Groove Binding, and Aggregation. Top Curr. Chem 2005, 253, 55–76.

(39). Hannah KC; Armitage BA DNA-Templated Assembly of Helical Cyanine Dye Aggregates: A Supramolecular Chain Polymerization. Acc. Chem. Res 2004, 37, 845–853. [PubMed: 15612674]

(40). Teo YN; Kool ET DNA-Multichromophore Systems. Chem. Rev 2012, 112, 4221–4245. [PubMed: 22424059]

(41). Knapp EW Lineshapes of Molecular Aggregates - Exchange Narrowing and Intersite Correlation. Chem. Phys 1984, 85, 73–82.

(42). Whittaker DM; Kinsler P; Fisher TA; Skolnick MS; Armitage A; Afshar AM; Sturge MD; Roberts JS Motional Narrowing in Semiconductor Microcavities. Phys. Rev. Lett 1996, 77, 4792–4795. [PubMed: 10062632]

(43). Bonifacio R; Lugiato LA Cooperative Radiation Processes in 2-Level Systems - Superfluorescence. Phys. Rev. A: At., Mol., Opt. Phys 1975, 11, 1507–1521.

(44). Bonifacio R; Lugiato LA Cooperative Radiation Processes in 2-Level Systems - Superfluorescence 2. Phys. Rev. A: At., Mol., Opt. Phys 1975, 12, 587–598.

(45). Marcus RJ; Haugen GR Resonance Fluorescence in Chlorophyll a Solutions. Photochem. Photobiol 1965, 4, 183–192.

(46). Herz AH Aggregation of Sensitizing Dyes in Solution and Their Adsorption onto Silver-Halides. Adv. Colloid Interface Sci 1977, 8, 237–298.

(47). Mobius D Scheibe Aggregates. Adv. Mater 1995, 7, 437–444.

(48). Malinovskii VL; Wenger D; Haner R Nucleic Acid-Guided Assembly of Aromatic Chromophores. Chem. Soc. Rev 2010, 39, 410–422. [PubMed: 20111767]

(49). Jelley EE Spectral Absorption and Fluorescence of Dyes in the Molecular State. Nature 1936, 138, 1009–1010.

(50). Jelley EE Molecular, Nematic and Crystal States of I: IDiethyl-Cyanine Chloride. Nature 1937, 139, 631–632.

(51). Scheibe G; Kandler L; Ecker H Polymerisation and Polymere Adsorption as a Cause of Novel Absorption Bands of Organic Pigments. Naturwissenschaften 1937, 25, 75–75.

(52). Scheibe G; Mareis A; Ecker H The Reversible Polymer-isation as a Cause of Unusual Absorption Bands III. Naturwissenschaften 1937, 25, 474–475.

(53). Scheibe G Über die Veränderlichkeit der Absorptionsspektren in Lösungen und die Nebenvalenzen als ihre Ursache. Angew. Chem 1937, 50, 212–219.

(54). Fujii T; Kashida H; Asanuma H Analysis of Coherent Heteroclustering of Different Dyes by Use of Threoninol Nucleotides for Comparison with the Molecular Exciton Theory. Chem. - Eur. J 2009, 15, 10092–10102. [PubMed: 19722239]

(55). Conley NR; Pomerantz AK; Wang H; Twieg RJ; Moerner WE Bulk and Single-Molecule Characterization of an Improved Molecular Beacon Utilizing H-Dimer Excitonic Behavior. J. Phys. Chem. B 2007, 111, 7929–7931. [PubMed: 17583944]

(56). Ogawa M; Kosaka N; Choyke PL; Kobayashi H H-Type Dimer Formation of Fluorophores: A Mechanism for Activatable, in Vivo Optical Molecular Imaging. ACS Chem. Biol 2009, 4, 535–546. [PubMed: 19480464]

(57). Nalbach P; Thorwart M Quantum Coherence and Entanglement in Photosynthetic Light-Harvesting Complexes In Quantum Efficiency in Complex Systems, Pt I: Biomolecular Systems; Weber ER, Thorwart M, Wurfel U, Eds.; 2010; Vol. 83, pp 39–75.

(58). Arndt M; Juffmann T; Vedral V Quantum Physics Meets Biology. HFSP J. 2009, 3, 386–400. [PubMed: 20234806]

(59). Fassioli F; Dinshaw R; Arpin PC; Scholes GD Photosynthetic Light Harvesting: Excitons and Coherence. J. R. Soc., Interface 2014, 11, 20130901. [PubMed: 24352671]

(60). Goodsell DS Biomolecules and Nanotechnology. Am. Sci 2000, 88, 230–237.

(61). Asanuma H; Fujii T; Kato T; Kashida H Coherent Interactions of Dyes Assembled on DNA. J. Photochem. Photobiol., C 2012, 13, 124–135.

(62). Markova LI; Malinovskii VL; Patsenker LD; Haner R Synthesis and Properties of Squaraine-Modified DNA. Org. Biomol. Chem 2012, 10, 8944–8947. [PubMed: 23076304]

(63). Kashida H; Asanuma H Preparation of Supramolecular Chromophoric Assemblies using a DNA Duplex. Phys. Chem. Chem. Phys 2012, 14, 7196–7204. [PubMed: 22532160]

(64). Kashida H; Tanaka M; Baba S; Sakamoto T; Kawai G; Asanuma H; Komiyama M Covalent Incorporation of Methyl Red Dyes into Double-Stranded DNA for Their Ordered Clustering. Chem. - Eur. J 2006, 12, 777–784. [PubMed: 16163760]

(65). Conley NR; Biteen JS; Moerner WE Cy3-Cy5 Covalent Heterodimers for Single-Molecule Photoswitching. J. Phys. Chem. B 2008, 112, 11878–11880. [PubMed: 18754575]

(66). Eisfeld A; Briggs JS The J-Band of Organic Dyes: Lineshape and Coherence Length. Chem. Phys 2002, 281, 61–70.

(67). Yang MN Influence of Energy Transfer on the Intensity Pattern of Vibronic Excitation Studied by Reduced Density-Matrix Theory. J. Mol. Spectrosc 2006, 239, 108–114.

(68). Womick JM; Moran AM Vibronic Enhancement of Exciton Sizes and Energy Transport in Photosynthetic Complexes. J. Phys. Chem. B 2011, 115, 1347–1356. [PubMed: 21268650]

(69). Schroter M; Ivanov SD; Schulze J; Polyutov SP; Yan Y; Pullerits T; Kuhn O Exciton-Vibrational Coupling in the Dynamics and Spectroscopy of Frenkel Excitons in Molecular Aggregates. Phys. Rep 2015, 567, 1–78.

(70). Polyutov S; Kuhn O; Pullerits T Exciton-Vibrational Coupling in Molecular Aggregates: Electronic versus Vibronic Dimer. Chem. Phys 2012, 394, 21–28.

(71). Kuhn O; Renger T; May V Theory of Exciton-Vibrational Dynamics in Molecular Dimers. Chem. Phys 1996, 204, 99–114.

(72). Thompson BJ; Camien MN; Warner RC Kinetics of Branch Migration in Double-Stranded DNA. Proc. Natl. Acad. Sci. U. S. A 1976, 73, 2299–2303. [PubMed: 1065879]

(73). Sha R; Liu FR; Seeman NC Direct Evidence for Spontaneous Branch Migration in Antiparallel DNA Holliday Junctions. Biochemistry 2000, 39, 11514–11522. [PubMed: 10985798]

(74). Panyutin IG; Biswas I; Hsieh P A Pivotal Role for the Structure of the Holliday Junction in DNA Branch Migration. EMBO J. 1995, 14, 1819–1826. [PubMed: 7737132]

(75). Panyutin IG; Hsieh P The Kinetics of Spontaneous DNA Branch Migration. Proc. Natl. Acad. Sci. U. S. A 1994, 91, 2021–2025. [PubMed: 8134343]

(76). Lushnikov AY; Bogdanov A; Lyubchenko YL DNA Recombination - Holliday Junctions Dynamics and Branch Migration. J. Biol. Chem 2003, 278, 43130–43134. [PubMed: 12949070]

(77). Seeman NC; Kallenbach NR DNA Branched Junctions. Annu. Rev. Biophys. Biomol. Struct 1994, 23, 53–86. [PubMed: 7919792]

(78). Seeman NC; Chen JH; Kallenbach NR Gel-Electrophoretic Analysis of DNA Branched Junctions. Electrophoresis 1989, 10 (5–6), 345–354. [PubMed: 2548837]

(79). Seeman NC; Kallenbach NR Design of Immobile Nucleic-Acid Junctions. Biophys. J 1983, 44, 201–209. [PubMed: 6197102]

(80). Seeman NC; Kallenbach NR Optimal-Design of Immobile and Semi-Mobile Nucleic-Acid Junctions. Biophys. J 1982, 37, A93–A93.

(81). Seeman NC Nucleic-Acid Junctions and Lattices. J. Theor. Biol 1982, 99, 237–247. [PubMed: 6188926]

(82). Kallenbach NR; Ma RI; Seeman NC An Immobile Nucleic-Acid Junction Constructed from Oligonucleotides. Nature 1983, 305, 829–831.

(83). Zwillinger D CRC Standard Mathematical Tables and Formulae, 31st ed.; CRC Press: 2002.

(84). Huang ZX; Ji DM; Wang SF; Xia AD; Koberling F; Patting M; Erdmann R Spectral Identification of Specific Photo-physics of Cy5 by Means of Ensemble and Single Molecule Measurements. J. Phys. Chem. A 2006, 110, 45–50. [PubMed: 16392838]

(85). Berova N; Nakanishi K Circular Dichroism: Principles and Applications; John Wiley & Sons: 2000.

(86). Couch GS; Hendrix DK; Ferrin TE Nucleic Acid Visualization with UCSF Chimera. Nucleic Acids Res. 2006, 34 (4), e29. [PubMed: 16478715]

(87). Pettersen EF; Goddard TD; Huang CC; Couch GS; Greenblatt DM; Meng EC; Ferrin TE UCSF chimera - A Visualization System for Exploratory Research and Analysis. J. Comput. Chem 2004, 25, 1605–1612. [PubMed: 15264254]

(88). Harada N; Nakanishi K Exciton Chirality Method and Its Application to Configurational Studies of Natural Products. Acc. Chem. Res 1972, 5, 257.

(89). Duckett DR; Murchie AIH; Lilley DMJ The Role of Metal-Ions in the Conformation of the 4-Way DNA Junction. EMBO J 1990, 9, 583–590. [PubMed: 2303044]

(90). Schelly ZA; Harward DJ; Hemmes P; Eyring EM Bonding in Dye Aggregates - Energetics of Dimerization of Aqueous Cobalt(II)-4,4′,4″,4‴-Tetrasulfophthalocyanine Ion. J. Phys. Chem 1970, 74, 3040–3042.

(91). Mooi SM; Keller SN; Heyne B Forcing Aggregation of Cyanine Dyes with Salts: A Fine Line between Dimers and Higher Ordered Aggregates. Langmuir 2014, 30, 9654–9662. [PubMed: 25073802]

(92). Mooi SM; Heyne B Size Does Matter: How To Control Organization of Organic Dyes in Aqueous Environment Using Specific Ion Effects. Langmuir 2012, 28, 16524–16530. [PubMed: 23145855]

(93). Kunzler J; Samha L; Zhang R; Samha H Investigation of the Effect of Concentration on Molecular Aggregation of Cyanine Dyes in Aqueous Solutions. Am. J. Undergrad. Res 2011, 9, 1–4.

(94). Nygren J; Svanvik N; Kubista M The Interactions Between the Fluorescent Dye Thiazole Orange and DNA. Biopolymers 1998, 46, 39–51. [PubMed: 9612138]

(95). Kumar CV; Turner RS; Asuncion EH Groove Binding of a Styrylcyanine Dye to the DNA Double Helix - The Salt Effect. J. Photochem. Photobiol., A 1993, 74, 231–238.

(96). von Berlepsch H; Boettcher C H-Aggregates of an Indocyanine Cy5 Dye: Transition from Strong to Weak Molecular Coupling. J. Phys. Chem. B 2015, 119, 11900–11909. [PubMed: 26244552]

(97). Chakraborty S; Bhattacharjee D; Soda H; Tominaga M; Suzuki Y; Kawamata J; Hussain SA Temperature and Concentration Dependence of J-Aggregate of a Cyanine Dye in a Laponite Film Fabricated by Langmuir-Blodgett Technique. Appl. Clay Sci 2015, 104, 245–251.

(98). Spano FC The Spectral Signatures of Frenkel Polarons in H-and J-Aggregates. Acc. Chem. Res 2010, 43, 429–439. [PubMed: 20014774]
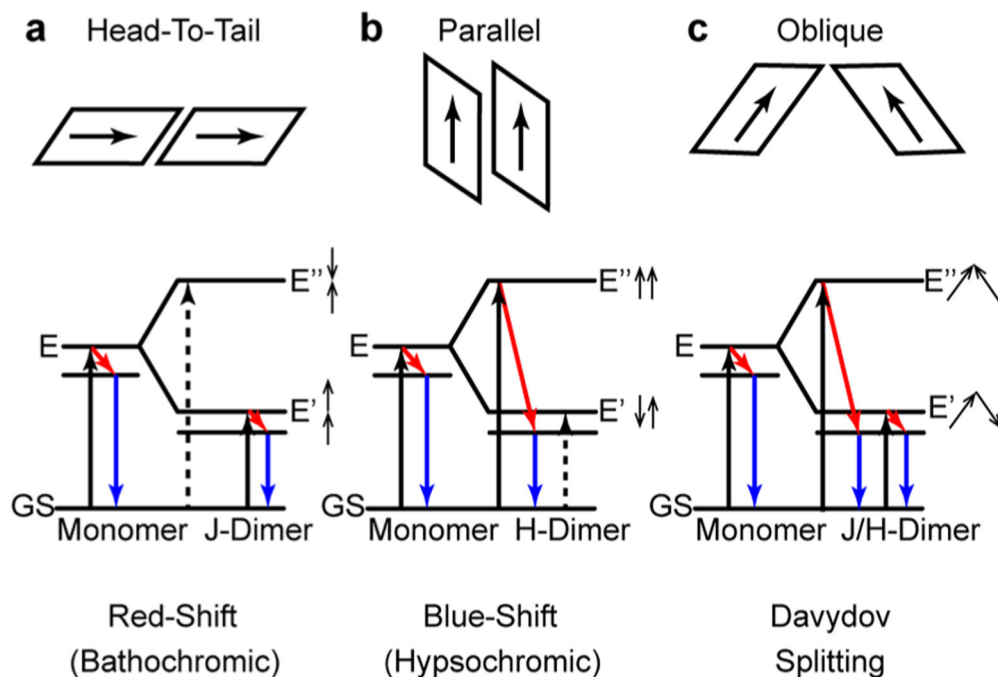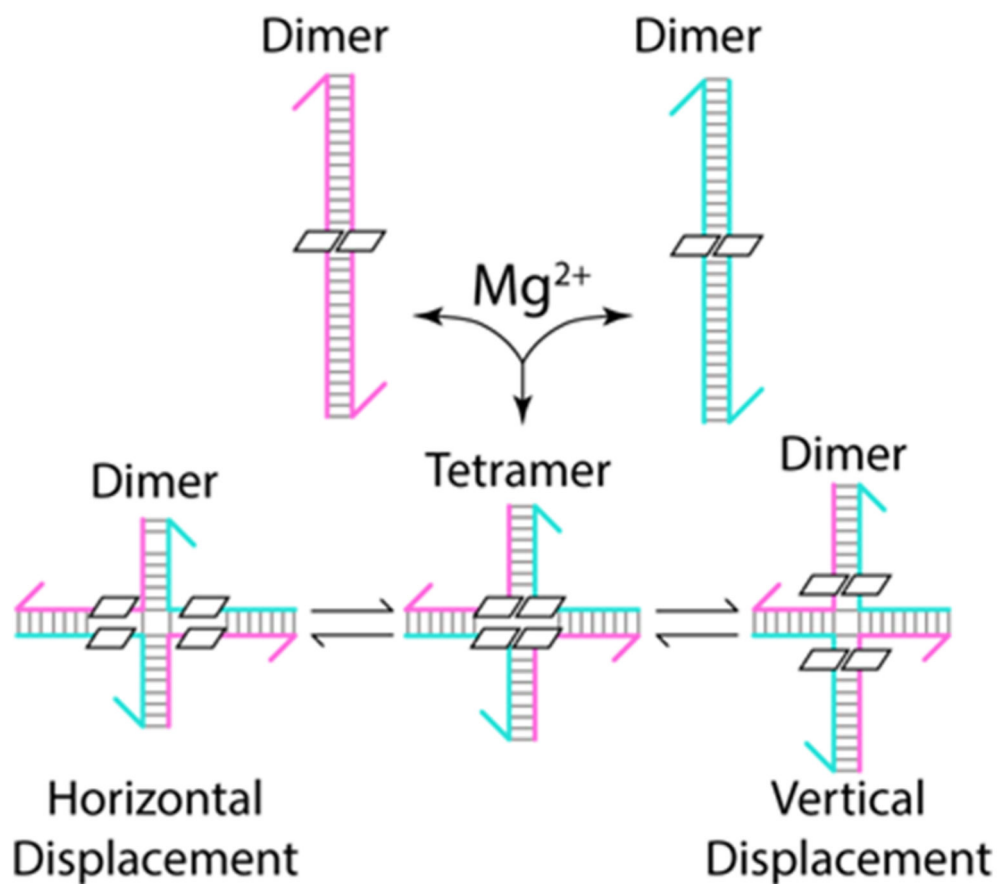
Figure 1.
Energy diagram illustrating the different excitation and relaxation pathways possible within (a) J-dimer, (b) H-dimer, and (c) oblique systems. Allowed absorption transitions are represented as solid black arrows, while dashed arrows indicate optically forbidden transitions. Blue and red arrows signify observed emission processes and nonradiative relaxation, respectively. The small arrows adjacent to each excited energy level represent the transition dipole moment of the corresponding molecules. Adapted from Kasha with permission.[14]
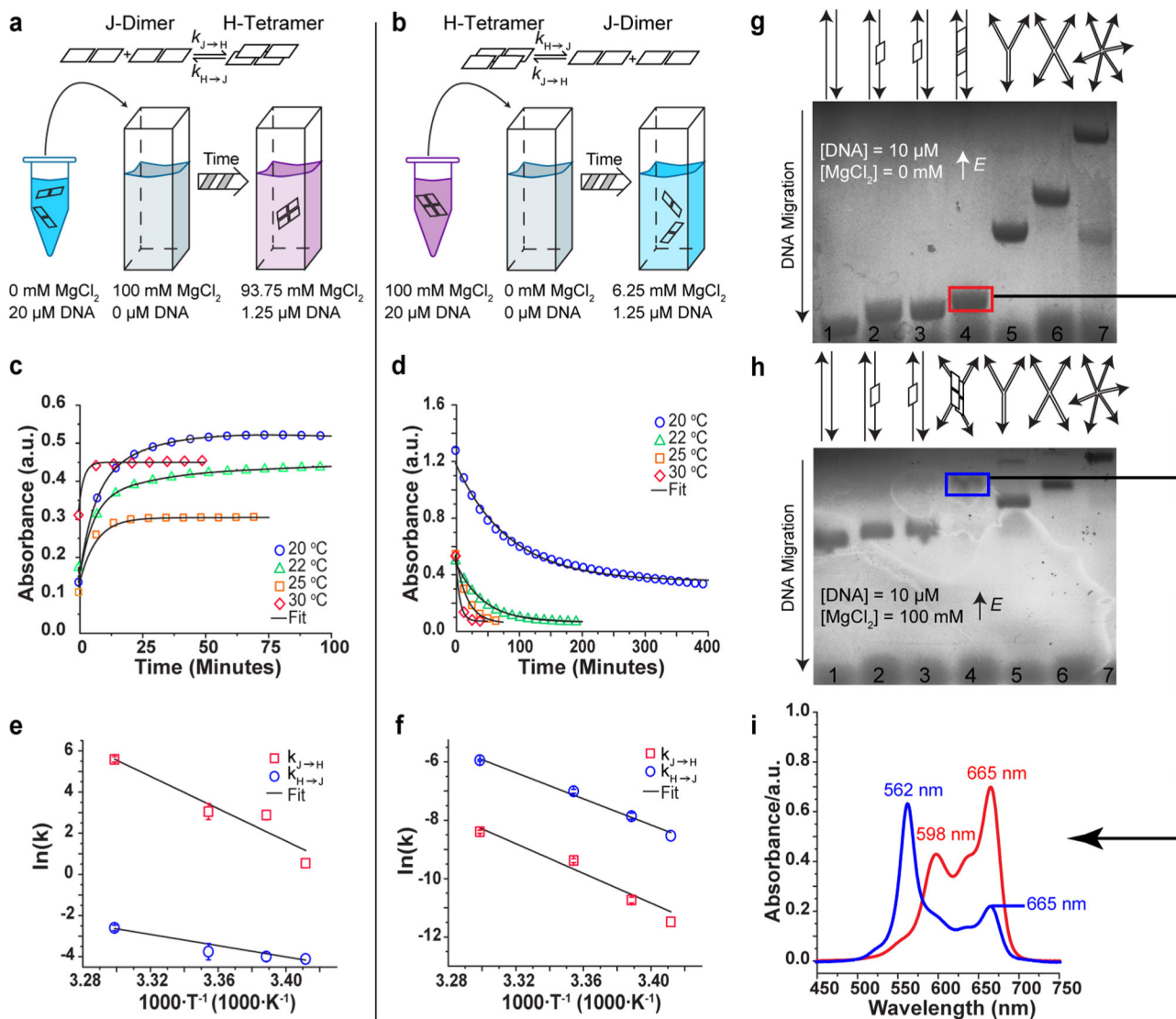
Figure 2.
Schematic illustration of the constituents of the two-state second-order reaction kinetics model in which two J-dimers couple together to form an H-tetramer through a four-way branch migration process. Also illustrated are the internal rearrangements within the core of the H-tetramer due to DNA breathing. As shown, dye dimers result when four-way branch migration steps cause the horizontal arms to become either longer or shorter than that of the dye tetramer, where all four dyes are located at the junction core.
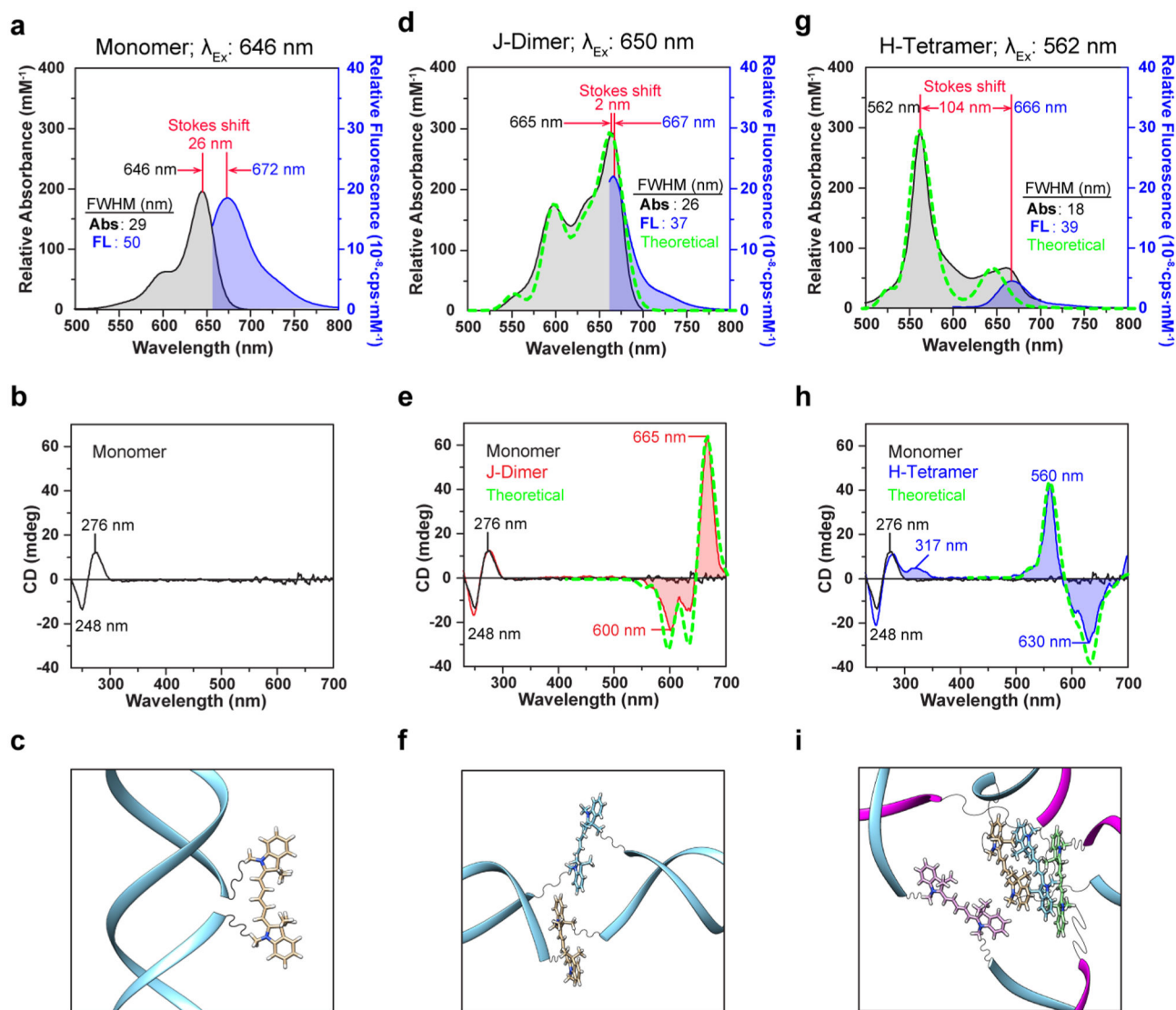
Figure 3.
(a) Relative visible absorbance (black traces and ordinate axes), fluorescence emission (blue traces and ordinate axes), and (b) CD spectra of the monomer (15 mM MgCl$_2$). (c) Illustration depicting one possible representation of a single Cy5 dye internally functionalized onto a DNA duplex. (d) Relative visible absorbance, fluorescence emission, and (e) CD spectra for the J-dimer (duplex, 0 mM MgCl$_2$). (f) Illustrative representation of the J-dimer stacked in a head-to-tail arrangement within a DNA duplex. (g) Relative visible absorbance, fluorescence emission, and (h) CD spectra of the H-tetramer (155 mM MgCl$_2$) stacking arrangements. (i) Illustrative representation of the H-tetramer formed within a four-armed DNA construct. Fluorescence spectra were acquired by exciting the dye constructs at their respective absorbance maxima. The FWHM of the absorbance (Abs) and fluorescence (FL) spectra were determined using a Gaussian fit, as described further in Supporting Information S5. Theoretical fits (green dashed curves) were produced using in-house software as described further in Supporting Information S2. All samples were prepared at 1.5 μM DNA concentrations.
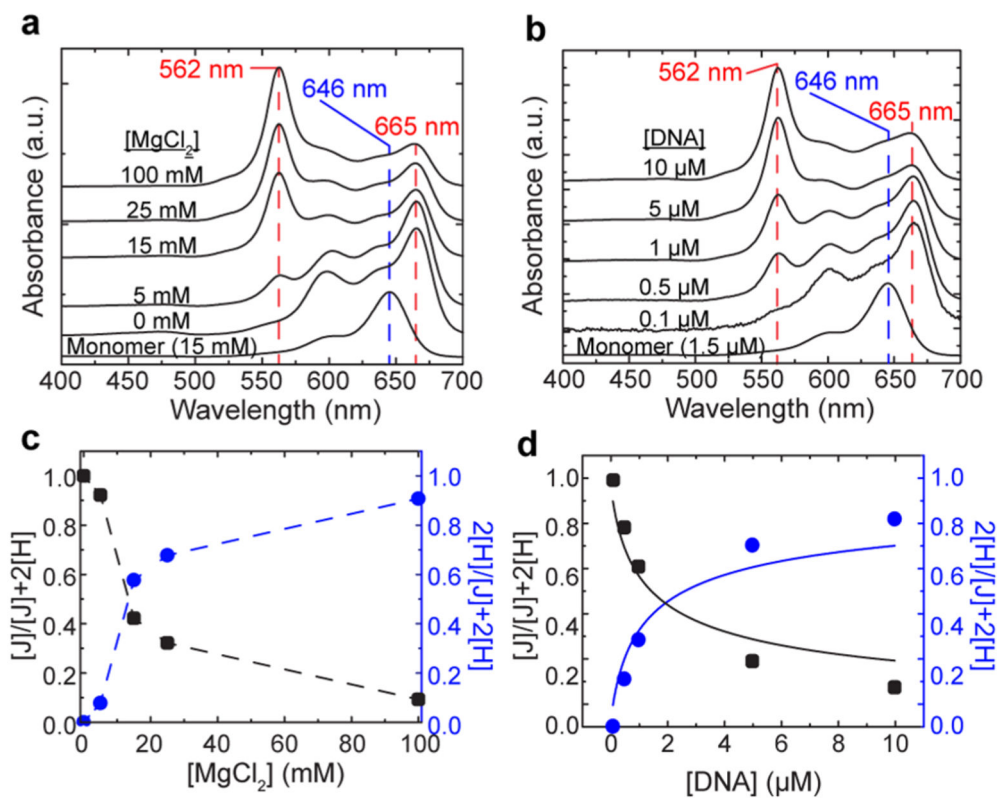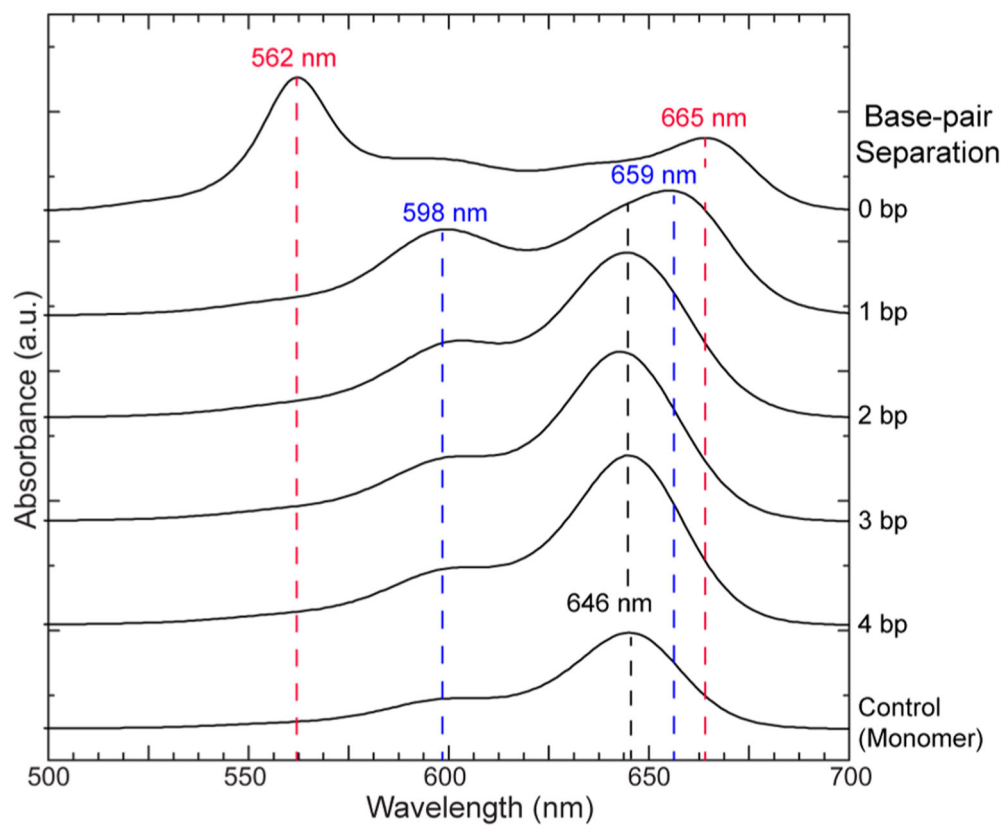
Figure 4.

Schematic illustrations of the reaction kinetics setup for solutions transitioning from (a) duplexes (J-dimers, 0 mM MgCl$_2$) to 4AJs (H-tetramers, 93.75 mM MgCl$_2$) and (b) 4AJs (H-tetramers, 100 mM MgCl$_2$) to duplexes (J-dimers, 6.25 mM MgCl$_2$). Initial dye–DNA solutions were prepared at DNA concentrations of 20 μM to yield final concentrations of 1.25 μM after dilution. Colors shown represent actual experimentally observed color changes. The depicted dye stacking arrangements are schematic representations and are not meant to imply specific geometric configurations. Corresponding reaction kinetics data of the time-dependent transitions: (c) J$_0$ → H93.75 (0 mM → 93.75 mM MgCl$_2$) and (d) H$_{100}$ → J$_{6.25}$ (100 → 6.25 mM MgCl$_2$). Shown are representative data sets fit to eq 14 using the averaged rate constant measured over multiple runs for a given temperature. The log of the averaged forward ($k_{J→H}$) and reverse ($k_{H→J}$) rate constants obtained from a total of three independent measurements are plotted versus the inverse temperature for (e) J$_0$ → H93.75 and (f) H$_{100}$ → J$_{6.25}$, respectively, to determine the activation energies of the forward

($E_{J\rightarrow H}$) and reverse ($E_{H\rightarrow J}$) reactions based on the best fit to the data (black line). Error bars were determined using the standard deviation. Structural characterization of the aggregates using electrophoresis to monitor the migration of (g) J- and (h) H-aggregates, prepared at 0 and 100 mM added $MgCl_2$, respectively, relative to a variety of DNA constructs (schematically represented). Absorbance spectra (i) of the excised and eluted bands were obtained for the J-dimer (red box) and the H-tetramer (blue box).

Figure 5.
Observed UV–vis absorbance spectra with varied (a) salt (DNA concentration held constant at 1.5 μM) and (b) DNA (added MgCl$_2$ concentration held constant at 15 mM) concentrations. Changes in J-dimer (black squares and ordinate axes) and H-tetramer (blue circles and ordinate axes) fractions (based on their respective absorbance peaks) as a function of (c) salt (i.e., MgCl$_2$) and (d) DNA concentrations. The dashed lines connecting the points in panel c are for visual aid only, while the curves in panel d were obtained by fitting the data according to eqs 19 and 20. Each spectrum was acquired at room temperature.

Figure 6.
UV–vis absorbance spectra documenting changes in the optical properties of the dye aggregate as the number of bps separating the dye pair is increased. Samples were prepared at 1.0 μM ds-DNA concentration with 15 mM $MgCl_2$ added. Spectra are normalized by DNA concentration.

Table 1.

Activation Energies ($E_{J \to H}$ and $E_{H \to J}$), Frequency Factors (A), and Free Energy (ΔG°) Values for Aggregation State Transitions

state	$E_{J \to H}$ (kJ/mol)	$E_{H \to J}$ (kJ/mol)	$A_{J \to H}$ (M^{-1} s^{-1})	$A_{H \to J}$ (s^{-1})	ΔG° (kJ/mol)
J_0–$H_{93.75}$	328.3 ± 7.3 (~3.4 eV)	211.6 ± 46.6 (~2.2 eV)	$(2.3 \pm 6.8) \times 10^{59}$	$(6.3 \pm 1.2) \times 10^{32}$	-22.5 (-0.23 eV)
H_{100}–$J_{6.25}$	113.8 ± 6.1 (~1.2 eV)	186.2 ± 41.8 (~1.9 eV)	$(2.5 \pm 7.3) \times 10^{18}$	$(3.5 \pm 5.9) \times 10^{28}$	7.1 (0.07 eV)